Changes in Electronic Structure upon Lithium Insertion into the A-Site Deficient Perovskite Type Oxides (Li,La)TiO_3

Masanobu Nakayama,[†,‡] Tatsuya Usui,[†] Yoshiharu Uchimoto,[†] Masataka Wakihara,*[,†] and Masahiro Yamamoto[§]

Department of Applied Chemistry, Tokyo Institute of Technology, Ookayama, Meguro-ku, Tokyo 152-8552, Japan, Japan Society for the Promotion of Science (JSPS), Tokyo, Japan, and Department of Energy and Hydrocarbon Chemistry, Kyoto University, Kyoto 615-8510, Japan

Received: August 31, 2004; In Final Form: November 24, 2004

Investigation on variation of the electronic structure accompanying the electrochemical lithium insertion into the perovskite type oxide, (Li,La)TiO_3, has been carried out by X-ray absorption spectroscopy (XAS). During the electrochemical lithium insertion, titanium ion reduced its oxidation state from Ti^{4+} to Ti^{3+}, while La^{3+} does not contribute to the reduction reaction resulting from Ti K-edge and La L_3-edge XAS, respectively. Furthermore, O K-edge XAS showed marked spectral changes with electrochemical lithium insertion, indicating the electronic structure around oxide ion affected by lithium insertion reaction. From the XAS measurement, we have concluded the variation observed in O K-edge XAS was related to the strong interaction with inserted Li ion. To confirm this, first-principles band calculations were performed for the perovskite structure before and after electrochemical lithium insertion. The calculated results showed that the electron originated from inserted Li transferred to neighboring oxide ion locally as well as to Ti ion. This may be due to local neutralization effect of Li to reduce the electrostatic interaction in the crystal.

1. Introduction

An increasing interest developed around transition-metal (TM) oxides with lithium insertion sites as the positive and the negative electrode materials for high energy density lithium ion batteries (LIB).[1,2] These materials are attractive enough not only to be used for the practical purposes but also to be employed as a model material in the fundamental study on solid-state electrochemical reaction. This stems from the two reasons described as follows: (1) the host crystal structure remained almost unchanged before and after the electrochemical reaction was proceeded; (2) the free energy of the reaction, the molar amount of reacted species, and kinetic parameters such as diffusion coefficient can be easily obtained by monitoring the cell voltage and electronic current. Therefore, materials prepared by electrochemical reaction are adequate enough to conduct treatment in experimental and theoretical manners, together with acquisition of useful knowledge, such as crystal and electronic structure at an equilibrium state, ion diffusion properties with the reaction, etc.[2]

Recently, it has been suggested that the electron-transfer accompanying the electrochemical lithium insertion occurs at oxide ions as well as TM ions using first principles calculation[3,4] and/or XAS technique.[5,6] This idea of the electron transfer at oxide ion is surprising because of being contrary to a conventional chemistry's point of view. (Usually TM ions solely contribute to the charge neutrality by redox reaction.) One of the reasons is the contribution of the hybridized orbital electrons, or covalent bond electrons, between TM d and oxygen 2p orbital to the electron-transfer reaction. From this viewpoint, the O 2p electron contribution to the electron transfer would be dominant with the increasing covalent character between TM and O. It has been well-known that the bond covalency can be estimated by the difference of electronegativity.[7,8] The larger difference in electronegativity, the stronger ionic bond was formed, and vice versa. Therefore, later TMs which have large electronegativity formed relatively strong covalent bond with oxide ions, and these materials showed significant contribution of the O 2p electron to the charge compensation reaction in the LIB.[7] Contrarily, early TMs with small electronegativity tend to show the ionic-bond character, and electron transfer is expected to occur mainly at the TM d orbital, not at the O 2p orbital. In other words, the O 2p contribution to the electron transfer process can be roughly estimated only by considering whether focused sample contains early TM or late TM. On the other hand, first-principles study by Van der Ven et al.[9] and XAS study by our group[10] indicated that the variation of electronic structure around oxide ion is induced by lithium ion itself. This indication is also surprising, because the Li 2s level is expected to be far from the Fermi energy where the electron transfer takes place.

In this paper, to reveal the origin of electron transfer at oxide ion, the electronic structure of A-site deficient type (Li,La)-TiO_3 was investigated by a combination of experimental and theoretical techniques, or XAS and first-principles calculation, respectively. The A-site deficient type perovskite oxides, (Li,La)TiO_3, would be suitable for fundamental studies on lithium insertion reaction due to the following reasons: (i) the material has a large number of vacancies to insert Li ions and (ii) there are two methods for lithium incorporation into $La_{2/3}TiO_3$ system—one is Li^+ substitution for La^{3+} (eq 2[11−16])

* Corresponding author. Tel.: + 81 3 5734 2145. Fax: +81 3 5734 2146.
† Tokyo Institute of Technology.
‡ JSPS.
§ Kyoto University.

10.1021/jp046062j CCC: $30.25
Published on Web 02/08/2005

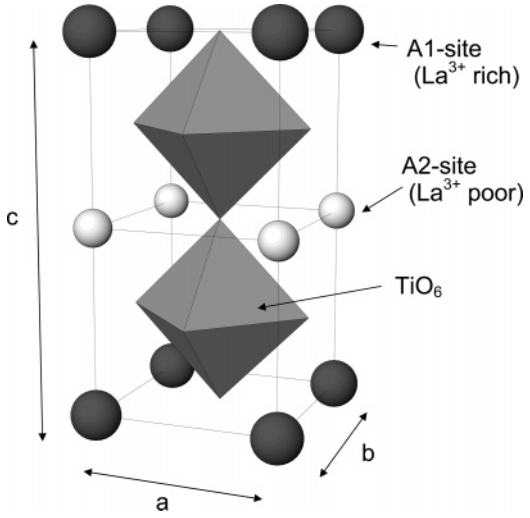

Figure 1. Crystal structure of $La_{2/3}TiO_3$.

and the other is electrochemical Li^+ insertion reaction (eq 1[17−19])

$$(y/2)Li_2CO_3 + [(2-y)/6]La_2O_3 + TiO_2 \rightarrow Li_yLa_{(2-y)/3}TiO_3 + (y/2)CO_2 \quad (1)$$

$$xLi^+ + xe^- + Li_yLa_{(2-y)/3}TiO_3 \rightarrow Li_{x+y}La_{(2-y)/3}TiO_3 \quad (2)$$

The reaction shown in eq 2 is classified as a redox reaction where Ti^{4+} ion is reduced to Ti^{3+} ion in classical sense. On the other hand, the reaction described in eq 1 does not accompany an electron transfer; the Ti^{4+} ion does not change its oxidation state. (Hereinafter in this paper, *x* means the molar composition of electrochemically inserted lithium ions, and *y* indicates the molar amount of substitution $3Li^+$ for La^{3+}.) In addition, the titanium ions belong to the early TM oxides, indicating typical example of TM oxide system which has the strong ionic bond. Therefore, it would be expected that the electron transfer upon lithium insertion reaction occur at Ti ion dominantly, if the electron transfer around oxide ion was induced solely by the concept of hybridization of TM-O orbital.

2. Structure Description

The crystal structure of $Li_yLa_{(2-y)/3}TiO_3$ has been already studied by many researchers (see such as ref 20), because this solid solution is known as a good ionic conductor of lithium ion (see such as ref 12). Figure 1 shows the crystal structure of (Li, La)TiO_3 based on the refs 13 and 16. La ions, Li ions, and vacancies are distributed in perovskite A-site and ordered within alternate (001) planes doubling the *c*-parameter of the primitive perovskite cell of ABO_3, and the structure lead to slightly distorted orthorhombic lattice (space group: *Pmmm*) with parameters $a \sim a_p$, $b \sim a_p$, $c \sim 2a_p$ (a_p refers to the cubic-perovskite type unit cell). In addition, it was observed that the crystal symmetry changed from orthorhombic (*Pmmm*) to tetragonal (*P*4/*mmm*) then to pseudocubic (the difference of lattice parameters *a* and *c* is quite small, but it still belongs to tetragonal *P*4/*mmm* symmetry) with increasing the lithium content in the perovskite structure. Such a structural change was ascribed to the disordering of A-site cations.[16] In addition to the alternative arrangement of La ions along *c*-axis, Inaguma et. al. recently reported that TiO_6 octahedron tilted along the *b* crystallographic axis in the perovskite system using neutron diffraction (space group belongs to *Cmmm* in this form).[21]

TABLE 1: ICP Analysis Data for $Li_yLa_{(2-y)/3}TiO_{3-\delta}$

starting composition	experimental composition	*y*
$Li_{0.09}La_{0.64}TiO_3$	$Li_{0.066}La_{0.64}TiO_{2.993}$	0.066
$Li_{0.14}La_{0.62}TiO_3$	$Li_{0.116}La_{0.62}TiO_{2.998}$	0.116
$Li_{0.20}La_{0.60}TiO_3$	$Li_{0.154}La_{0.60}TiO_{2.977}$	0.154
$Li_{0.29}La_{0.57}TiO_3$	$Li_{0.242}La_{0.57}TiO_{2.976}$	0.242
$Li_{0.35}La_{0.55}TiO_3$	$Li_{0.275}La_{0.55}TiO_{2.963}$	0.275
$Li_{0.45}La_{0.52}TiO_3$	$Li_{0.317}La_{0.52}TiO_{2.938}$	0.317

3. Experimental Section

Different compositions of the $Li_yLa_{(2-y)/3}TiO_3$ solid solution were prepared by conventional solid-state reaction. The mixture of stoichiometric amounts of Li_2CO_3, La_2O_3, and TiO_2 was heated at 800 °C for 2 h and then at 1300 °C for 12 h in air with several intermittent grindings. The molar ratio of the metals in the products was determined by inductive coupled plasma (ICP) spectroscopy. Crystalline phase identification and the evaluation of lattice parameters were carried out by powder X-ray diffraction using a Rigaku RINT2500V diffractometer with Cu*K*α radiation and a curved graphite monochromator.

Electrochemical reaction of Li insertion was carried out using a three-electrode cell. Li foil (Aldrich) was used as counter and reference electrodes and 1M solution of $LiClO_4$ in anhydrous propylene carbonate (PC) was used as electrolyte (Tomiyama Pure Chemical Company, Limited). The working electrode was the mixture of 90 wt % perovskite powders, 7 wt % acetylene black as a current collector, and 3 wt % poly(tetrafluoroethylene) (PTFE) binder. Li foils and the mixture of working electrode were pressed onto Ni mesh. Electrochemical lithium behavior was investigated by slow speed liner potential sweep method (0.05 mV/s) and interrupted galvanostatic method (current density; 40μA/cm^2 with relaxation time of 8 h) using Solartron 1287 and Hokuto HD-110mSM6 electrochemical interface, respectively.

The crystal and electronic structure of Li_x(Li,La)TiO_3 prepared by electrochemical reaction were investigated by XRD and XAS technique. The synthesis of the samples for XRD and XAS with various composition x was performed by electrochemical reaction with slow current density, 40 μA/cm^2, and relaxed to the state in equilibrium (>12 h). The crystalline phase identification was carried out by powder X-ray diffraction using Cu*K*β radiation. The samples were covered by polyethylene film in an Ar-filled glovebox to prevent reactions with moisture. The Ni powder was used as the internal standard for the correction of peak shift. The XAS measurements for the La L_3-edge, Ti K-edge spectra were carried out by transmission mode using synchrotron radiation at the beam line BL-7C, Photon Factory, High Energy Accelerator Research Organization in Tsukuba, Japan. The absorption of Cu K-edge was used for the calibration of the absolute energy scale. The pellets of samples after electrochemical treatment were sealed in polyethylene bag to avoid exposure in the air. The XAS measurements of O K-edge spectra were carried out using synchrotron radiation at the beam line BL-8B1, UVSOR, Institute for Molecular Science in Okazaki, Japan, respectively. The absorption was determined by the total-electron-yield method. The total yield was divided by the storage-ring current recorded simultaneously. For the samples after electrochemical treatment, all installation operations were performed under Ar or N_2 atmosphere.

4. Results and Discussion

Phase Identification of $Li_yLa_{(2-y)/3}TiO_{3-\delta}$. The chemical formula of $Li_yLa_{(2-y)/3}TiO_{3-\delta}$ determined by the ICP spectroscopy is given in Table 1. About 20% of initial amount of lithium

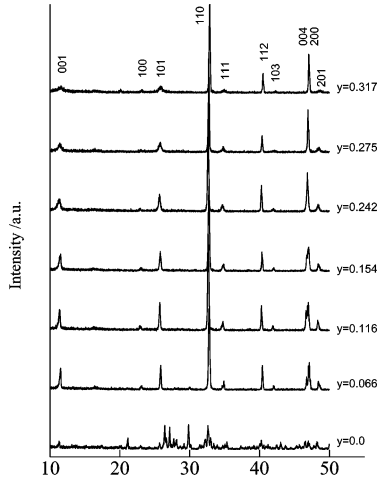

Figure 2. Powder X-ray diffraction patterns of $Li_yLa_{(2-y)/3}TiO_{3-\delta}$.

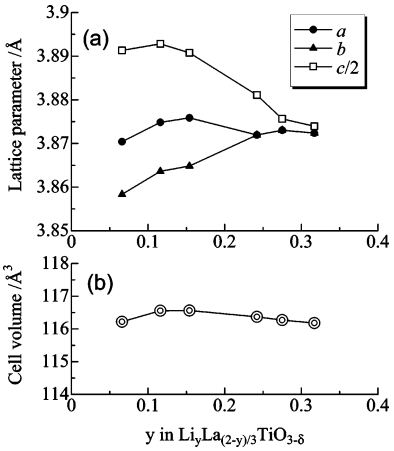

Figure 3. Variation of the (a) lattice parameters and (b) cell volumes versus composition y in $Li_yLa_{(2-y)/3}TiO_{3-\delta}$.

ions was lost due to the evaporation during sintering process, and the results were consistent with previous reports.[12] Figure 2 shows the XRD diagrams for $Li_yLa_{(2-y)/3}TiO_{3-\delta}$ ($0.0 \leq y \leq 0.317$). The only perovskite phase was observed in the composition range from $y = 0.066$ to 0.317. On the other hand, the $La_{2/3}TiO_3$ ($y = 0$) showed impurity phase under our experimental condition, showing the same result as the previous research.[22] Figure 3a,b represents the variation of lattice parameters and cell volumes for $Li_yLa_{(2-y)/3}TiO_{3-\delta}$. The cell volumes are almost constant, while the decrease in the orthorhombic distortion was observed as a function of y in $Li_yLa_{(2-y)/3}TiO_{3-\delta}$. It would be ascribed to the disordering of A-site cations as mentioned in previous section, because the intensity of (001) peak arising from the A-site cation ordering along *c*-axis were disappearing with composition y.[11, 12, 16]

Electrochemical Lithium Insertion into $Li_yLa_{(2-y)/3}TiO_{3-\delta}$. The slow-speed liner sweep voltamograms upon the electrochemical lithium insertion are shown in the Figure 4, and three cathodic peaks denoted by peaks 1 to 3 in the figure were observed roughly at ~1.5, ~1.1, and ~0.7 V, respectively. Considering our previous study,[10] the peak less than 1 V (Peak3) would be ascribed to the lithium insertion into acetylene black. Figure 5 shows the relaxed potential diagrams during the electrochemical Li insertion by interrupted galvanostatic method at $x = 0.01$ intervals. The value x_1 in the Figure 5 is the composition where the potential curve is bended, and its potential showed good accordance with that of the first peak end in the voltamograms (shown as arrow between Peak1 and

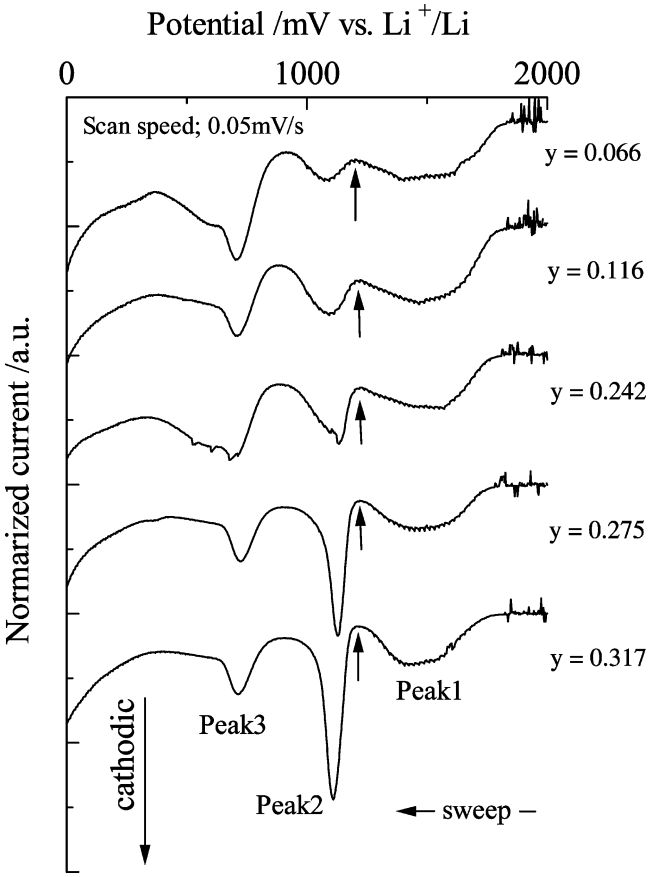

Figure 4. The slow speed liner potential sweep measurement for $Li_yLa_{(2-y)/3}TiO_{3-\delta}$. Arrows between peak1 and 2 indicate the potential where the first lithium insertion process terminated.

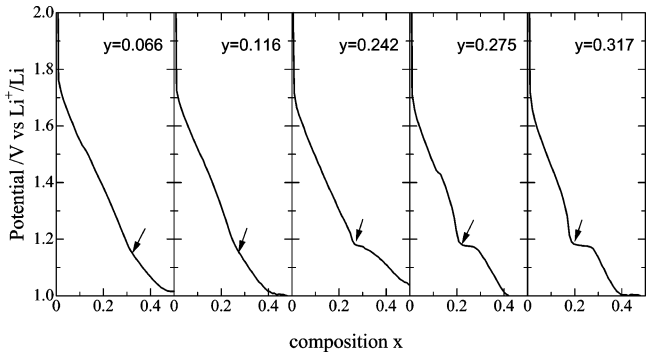

Figure 5. Quasi open circuit voltage with composition x in $Li_xLi_yLa_{(2-y)/3}TiO_{3-\delta}$. Arrows indicate the composition x_1 where the first lithium insertion process terminated (see Figure 4).

TABLE 2: Compositional Dependence of (a) the Amount of Vacancy Site Based on the Data Listed in Table 1 and (b) the Amount of Inserted Lithium Ions upon the First Step (Composition x_1)

y	number of vacancy site$_{/Li_yLa_{(2-y)/3}TiO_{3-\delta}}$	number of inserted lithium ions for the first step/$Li_yLa_{(2-y)/3}TiO_{3-\delta}$
0.066	0.293	0.32
0.116	0.264	0.26
0.242	0.246	0.25
0.275	0.175	0.20
0.317	0.163	0.18

Peak2 in Figure 4). Since the composition x_1 is almost equal to the total amount of A-site vacancies (Table 2), peak 1, ~ 1.5 V, is related to the electrochemical reaction into perovskite A-site vacancies. Shan et al. [17] reported previously the lithium

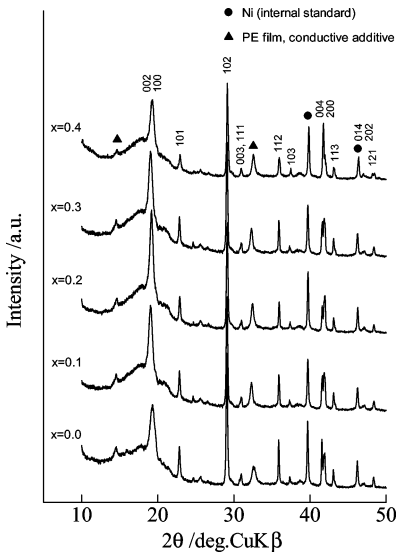

Figure 6. Powder X-ray diffraction patterns of $Li_xLi_{0.066}La_{0.64}TiO_{2.993}$.

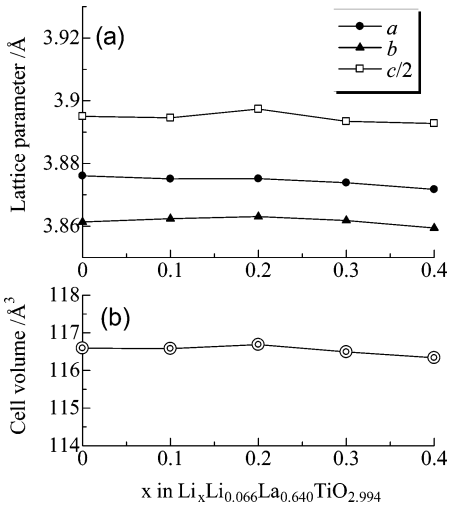

Figure 7. Comparison of the slow speed liner potential sweep measurement for $Li_xLi_{0.066}La_{0.640}TiO_{2.994}$.

insertion mechanism of perovskite oxides, $La_{0.50}Li_{0.37}TiO_{2.94}$, and concluded that the lithium ions are initially inserted into A-site vacancy and then into 3c-site (the center position between two A-sites). Hence peak 2 would be ascribed to lithium insertion into the 3c-site. However, the direct evidence of lithium location during peak 2 reaction is not clarified yet, mainly due to the experimental difficulty caused by the low X-ray scattering ability of lithium ion. In addition, peak 2 in Figure 4 tended to sharpen with composition *y*; however, the exact reason is still uncertain. Therefore, we mainly discuss the well-defined electrochemical behavior of peak 1 hereinafter in this paper.

Figures 6 and 7 show the variations of powder XRD patterns and observed lattice parameters for the samples prepared by electrochemical Li insertion, $Li_xLi_{0.066}La_{0.640}TiO_{2.994}$. The peak feature of the patterns was roughly unchanged with Li insertion, indicating the host structure keeps its framework upon Li insertion. The lattice parameters also do not show the significant change during the electrochemical lithiation, indicating that the lattice expansion/shrinkage effect would hardly affect the compositional dependence of electrochemical behavior.

Summing up the electrochemical behavior, the lithium insertion reaction occurs stepwise in the Perovskite samples, and the first step of the reaction around 1.5 V is corresponds to the Li insertion into A-site defect.

X-Ray Absorption Spectroscopy. The results of the XAS measurements for the samples of electrochemical lithium insertion are shown in Figure 8. La L_3-edge XAS (Figure 8a) shows no noticeable change, indicating that the oxidation states of La ions at A-site are unchanged through the reaction. The Ti K-edge XAS around absorption edge for the samples, $Li_xLi_{0.066}La_{0.640}TiO_{2.994}$, is shown in Figure 8b, and absorption edge of the Ti K-edge XAS shifted gradually to the lower energy side with electrochemical lithiation. Hence, the Ti ion reduced its oxidation state from +4 toward +3. In addition, three peaks were observed in the preedge region around 4970 eV of Ti K-edge XAS, which shows the transitions to the Ti 3d level and tended to broaden with composition x. Since the Ti 1s-to-3d transition is forbidden according to the Fermi Golden rule, the preedge absorption would reflect the hybridization of the Ti 3d and O 2p orbital. Therefore the broadening of the peaks would correspond to the decrease in covalent character between Ti and O ions. Figure 8c shows the O K-edge spectra of the samples with composition *x*. Considering the selection rule for the absorption spectra, the peaks should assign as O 2p conduction band consisting of Metal-Oxide hybridization orbital. In Figure 8c, the spectra can be divided into two regions at 535 eV. The region above 535 eV, rather broad peaks were observed, and it was generally known that these peaks corresponded to the O 2p orbital hybridized with transition metal 4sp orbital.[5,6,8,9] On the other hand, the peaks at the region less than 535 eV are relatively sharp (indicating localized electron orbital, such as d character) and changing with insertion. Therefore, the absorption peaks would be ascribed to the hybridized orbital between Ti 3d and O 2p state (and/or La 5d and O 2p). Three peaks (a−c) were observed at the composition $x = 0$ in the range from 525 to 535 eV. However, peaks a and c disappeared with electrochemical Li insertion, and peak b sharpened gradually at about 532 eV. Therefore, it is confirmed that the electronic structure of oxide ion changes with Li insertion reaction as observed in previous researches.[8,9] The conclusion is rather surprising, because the Ti−O bond has been thought to form strong ionic one, or electron-addition state due to electrochemical lithiation is not Ti−O hybridization orbital but primarily Ti 3d orbital as mentioned in Introduction section. However, the results clearly show the existence of some electronic structure effects around oxide ion during the electron transfer in electrochemical reaction.

The electronic structure of oxide ion would be affected by the interaction of neighboring cations, and there are three kinds of cations interacting with oxide ion, Ti at perovskite B-site and La and Li at perovskite A-site. It is considered that the interaction between La and O does not affect the changes of electronic structure of oxide ions, because the electronic structure of La ions does not change with Li insertion as shown in Figure 8a. Hence, the changes of electronic structure of oxide ions will be explained by two hypotheses. The first is that the changes of the interaction of Ti−O, or that of oxidation state in titanium ions (Figure 8b), affects the electron orbital of neighboring oxide ions. From the following discussion on the first principles calculation, the bond between titanium and oxygen has rather covalent character than that of Li−O and La−O. Therefore, such a change of O K-edge spectra corresponds to the electron transfer occurred at Ti−O hybridized orbital during the electrochemical reaction, or the oxide ions also contribute to the reduction reaction. This hypothesis indicates Ti−O in the perovskite oxides forms strong covalent bond rather than the pure ionic one which was expected generally. The other hypothesis is focused on the effect of Li−O interaction. Usually it was thought that the Li 2s orbital level is quite higher than

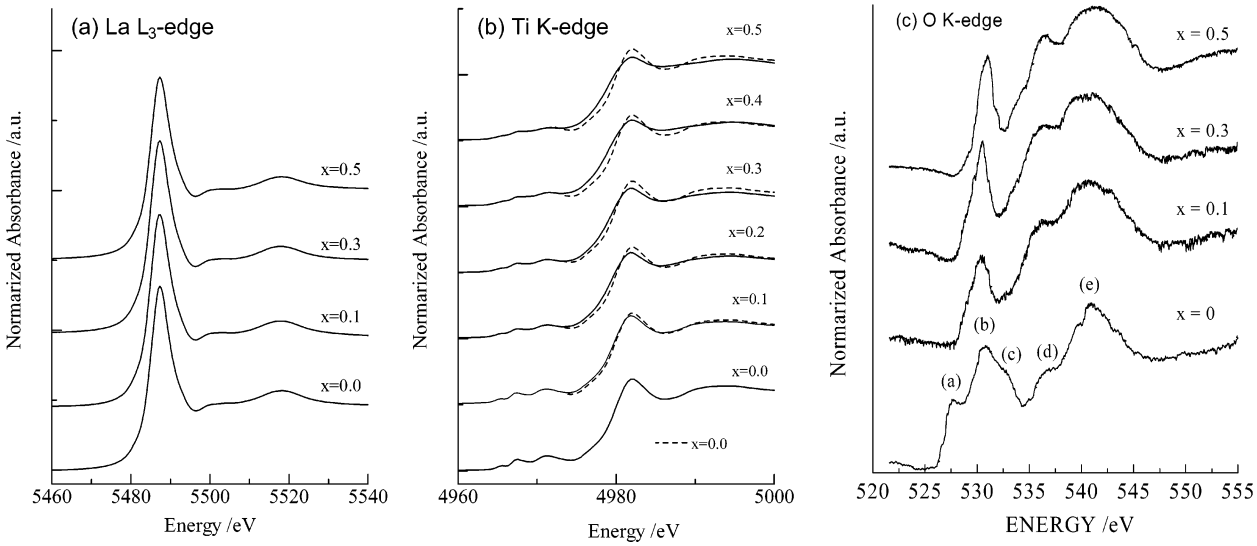

Figure 8. The variation of lattice parameters with composition x in $Li_xLi_{0.066}La_{0.640}TiO_{2.994}$. (a) La L_3-edge, (b) Ti K-edge (hatched line indicates the sample with composition $x = 0$ for the comparison of edge energy), and (c) O K-edge.

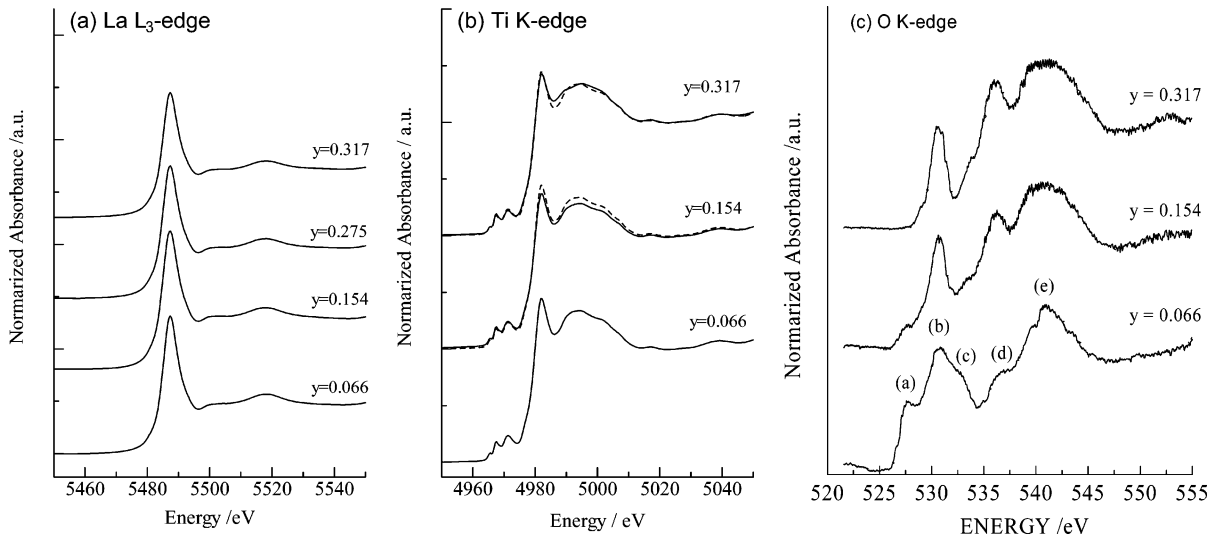

Figure 9. The variation of lattice parameters with composition y in $Li_yLa_{(2-y)/3}TiO_{3-\delta}$. (a) La L_3-edge, (b) Ti K-edge (hatched line indicates the sample with composition $x = 0$ for the comparison of edge energy), and (c) O K-edge.

Fermi level, and lithium ion would not affect directly the electronic structure around energy region observed in the O K-edge absorption edge. However, the lithium ion is known by having strong ionic character; hence it is considered that the Coulombic field varies around insertion site and causes the electronic structural change of neighboring oxide ions.

To clarify the mechanism of the changes in O K-edge spectra, we investigated the XAS of the samples with Li^+ substitution for La^{3+}. Figure 9 shows the XAS as a function of y in $Li_yLa_{(2-y)/3}TiO_{3-\delta}$. As seen in the figure, the La L_3-edge and Ti K-edge were unchanged with composition *y*. Note that in this system, it was expected that the net redox reaction did not occur (see eq 2; Ti ions keep their formal oxidation state as +4 through the lithium insertion). Therefore, the unaltered spectra would reflect that unchanged nature in electronic structure took place during Li substitution for La as expected, and Ti is not affected by Li^+ ion content in the structure but is affected by the electron content. This indication is also supported by ^7Li NMR experiments reported by Emery et al.[23] In this report, it was revealed that no direct evidence was observed between the presence of ^7Li nuclei and the inserted electrons into perovskite accompanying electrochemical Li insertion. On the other hand, the O K-edge spectra (Figure 9c) varied with replacement of Li^+ without electron-transfer process and showed similar spectra to XAS of the samples with electrochemical Li^+ insertion (Figure 8c). Thus, O spectra are linked to the strong interaction with Li+ ion independently of the way this ion is introduced in the structure regardless of electron transfer at Ti ions. Accordingly, the origin of variation of electronic structure around oxide ions is ascribed to the second hypothesis, or some interaction (maybe a Coulombic one) between lithium ion and oxide ion affected to the spectral change as indicated by previous papers.[9,10]

First-Principles Calculations. First-principles calculations based on density functional theory (DFT) [24] for the model cell, $La_{2/3}TiO_3$ (VLTO; $La_4Ti_6O_{18}$) and $Li_{1/3}La_{2/3}TiO_3$ (LLTO; $Li_2La_4Ti_6O_{18}$), were carried out to investigate the electron-transfer process during the electrochemical reaction eq 1.

The first-principles calculation was done using all-electron full potential linearized augmented plane wave (FLAPW) method.[25] We have used the generalied gradient approximation (GGA)[26] for the exchange-correlation interaction. The program code Wien2k was employed.[27] For the simplification, the lattice parameters for the calculation were fixed, and we use the lattice

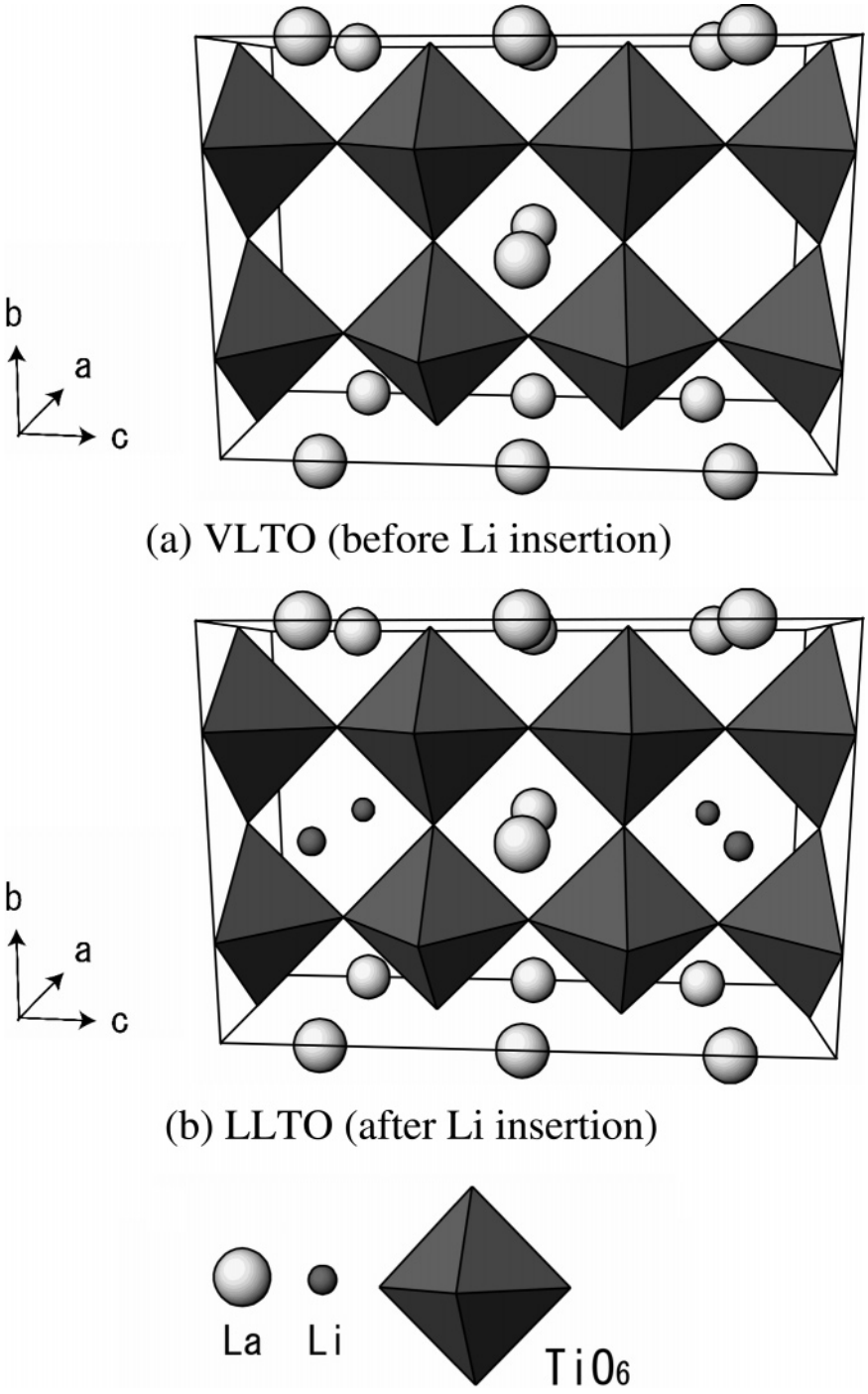

Figure 10. The crystal structure for the first-principles calculation: (a) VLTO and (b) LLTO.

parameters determined from the extrapolation of Figure 3. Figure 10 and Table 3 show the model cell before and after lithium insertion reaction (VLTO and LLTO). As mentioned above, the crystal structure of (Li,La)TiO_3 system belongs to tetragonal or orthorhombic symmetry (space group, *Pmmm*, *P*4/*mmm*, or *Cmmm* is suggested), and synthesis of $La_{2/3}TiO_3$ is difficult in the air. However, cubic-like structural model (see Table 3) was adopted this time to simplify the computational procedure, since it is beyond our computational resources that decreasing the symmetry operation and introducing the small amount of *y*, which require a large numbers of perovekite unit lattices. In our previous paper,[10] experimental XAS of the perovskite $La_{1/3}NbO_3$ roughly reproduced by the computational XAS within multiple-scattering theory under cubic-like model, indicating the major feature of XAS do not affected by the structural details. In addition, since the changes of cell volume is negligible small (Figure 7), the calculations before and after Li insertion were carried out under the assumption of the constant volume reaction, or both of the cell have the same lattice parameters. In this cell model, oxide ions are classified into eight crystallographic positions, labeled as O1 to O8, respectively (see Table 3). Integration in the reciprocal space was done using a $3 \times 6 \times 9$ mesh in the first Brillouin zone, and spin polarized DFT is used in this study. It was known that DFT within local density approximation (LDA) and GGA gives remarkably good agreement with experiments for many TM oxide electrodes systems of lithium ion battery.[28] However, note that perovskite $LaTiO_3$ is a Mott−Hubbard insulator, indicating that large Coulombic on-site effects lead to the failure in first-principles calculation within LDA/GGA.[29−33] Therefore, it may be plausible that

TABLE 3: Crystal Structure of VLTO and LLTO for the First Principles Calculation

VLTO and LLTO space group: *Pmmm* (No. 47) Lattice parameters: $a = 3.879$, $b = 7.758$, $c = 11.637$ /Å, $\alpha = \beta = \gamma = 90^\circ$.				
		fractional coordinates		
label/atom	no. of sites	*x*	*y*	*z*
La1/La	1	0	0.5	0.5
La2/La	2	0	0	1/6
La3/La	1	0	0	0.5
Ti1/Ti	4	0.5	0.2 5	1/3
Ti2/Ti	2	0.5	0.2 5	0
O1/O	4	0.5	0.2 5	1/6
O2/O	4	0	0.2 5	2/3
O3/O	2	0.5	0.2 5	0.5
O4/O	2	0	0.2 5	0
O5/O	2	0.5	0	1/3
O6/O	1	0.5	0	0
O7/O	2	0.5	0.5	1/3
O8/O	1	0.5	0.5	0
Li1/Li[a]	2	0	0.5	1/6

[a] Only used for the calculation of LLTO.

present DFT for the materials of VLTO and LLTO does not reproduce their accurate electronic structure. However, as a first approximation, DFT consideration was adapted to reveal the variation of electronic distribution around oxide ion during the electrochemical reaction.

The calculated local density of state (LDOS) for each ion is shown in Figure 11 (the Fermi energy level was shifted to zero). The LDOS of VLTO and LLTO indicated that the valence band was mainly composed of O 2p orbital, while the conduction band was mainly formed by Ti 3d orbital. The Li 2s level in the LLTO resides in the energy region higher than 6 eV from Fermi energy, indicating the lithium is completely ionized to Li^+. As seen in the figure, the shape of LDOS for oxygen seems to be related to that for titanium, on the other hand, the LDOS of La and Li ion was independent to the others. Therefore, Ti and O orbital would form relatively larger covalent contribution in their chemical bond, while La and Li would show the ionic bond character in the perovskite. This indication is similar to the recent report on the molecular dynamics simulation of (Li,La)TiO_3 system by Katsumata et al. where they argued that covalent bonding effect is crucial to reproduce the ionic conduction behavior.[34] It was also noted that band gap E_g (difference between top of the valence band and bottom of the conduction band) increased upon Li uptake. Hence the ionic character of perovskite the may be increased by the introduction of lithium. (Note that DFT band calculations usually tend to underestimate the band gap, however the general tendency of the variation in DOS indicates increase in band gap.)

Figure 12 shows the electron density distribution for VLTO and LLTO lattice. From the Figure 12a,b, chemical bonds between Ti and O ions showed stronger covalency than those between A-site cations (La, Li) and oxide ions. Figure 12c exhibits the positive part of electron-density difference between LLTO and VLTO. As shown in the figure, increase in electron density clearly observed at the Ti site, indicating Ti reduced its oxidation state during electrochemical reaction. On the other hand, no significant change in electron density around La is indicated, showing the La ion does not contribute the redox reaction, and it is consistent with the experimental results (Figure 8a). The increase in electron density around oxide ion varies with their crystallographic position (O1 to O8). As shown in Figure 12c, the differential electron density of the oxide ion near the lithium insertion site (for example O1 site shown in Figure 12c) shows larger increase than that of the oxide ion apart from lithium insertion site (e.g., the O3 site). Hence, the increase in electron around oxide ion is strongly related to the neighboring lithium ions, not to the titanium ions. For the quantitative discussion on this matter, the increase in electron as a function of integration radius is presented in Figure 12.

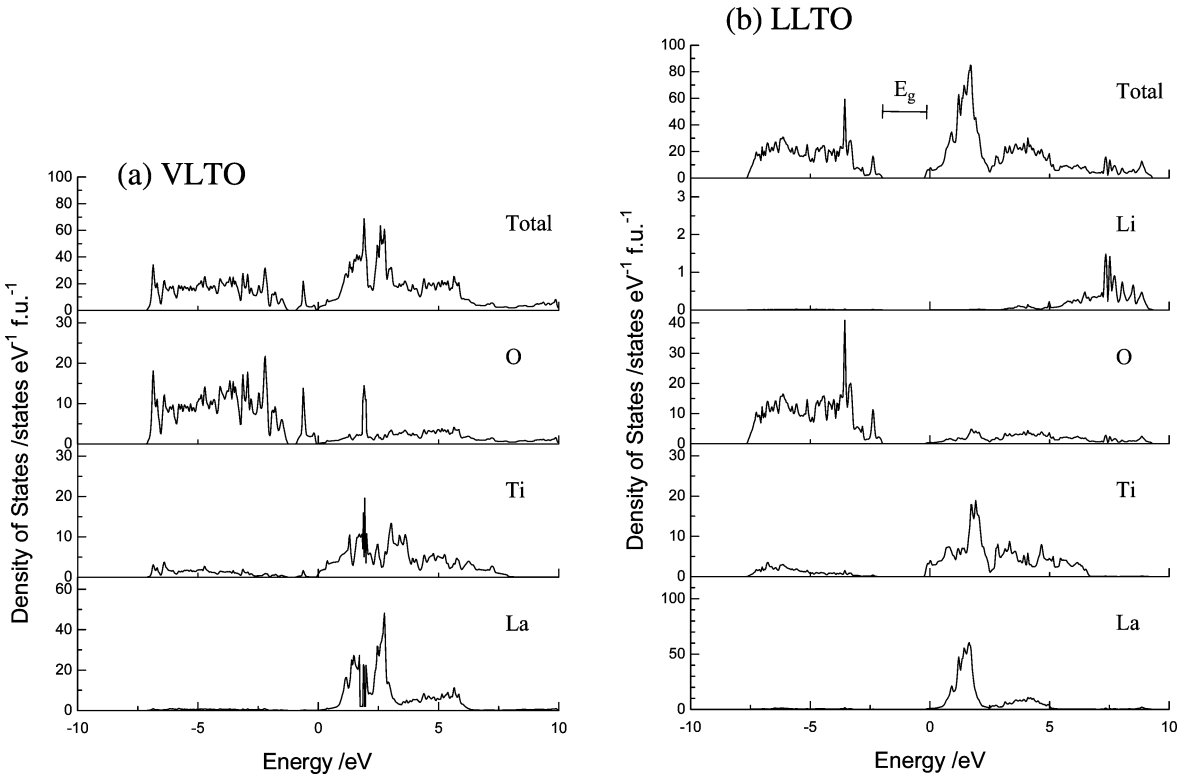

Figure 11. The calculated DOS and LDOS for (a) VLTO and (b) LLTO.

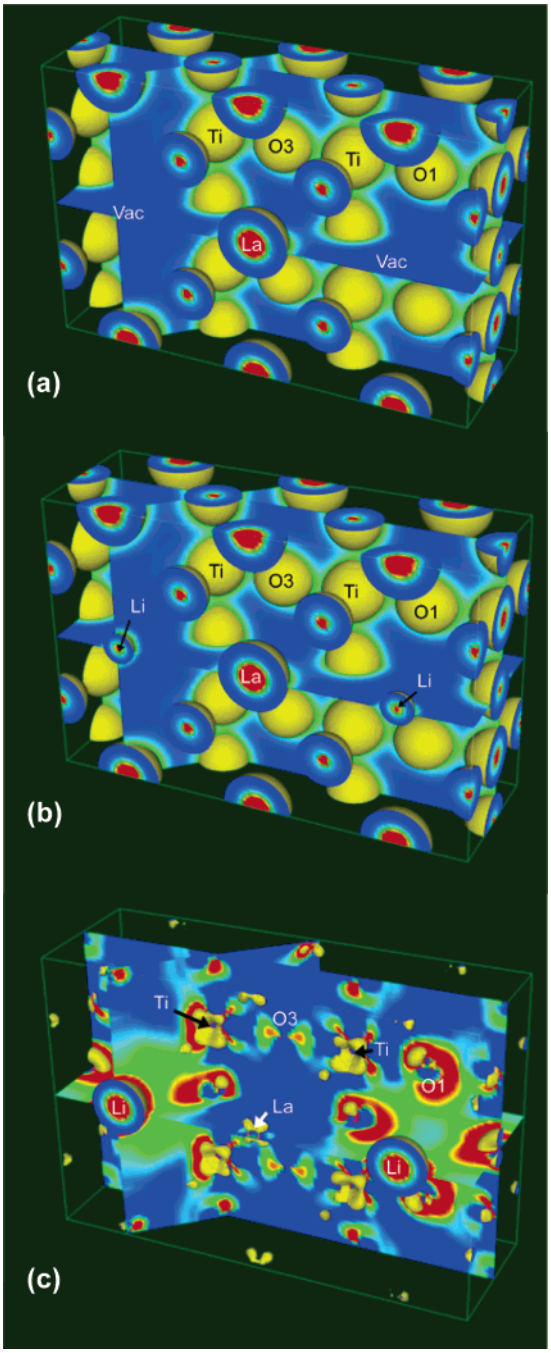

Figure 12. The calculated electron density for (a) VLTO, (b) LLTO, and (c) the positive area of the differenced in electron density before and after lithium insertion.

The increase in electron around oxide ion depends on the crystallographic site as mentioned above. For example, the electron density of O1 site showed larger increase than that of O3 site, which agrees with the results of Figure 11c. Figure 14 shows the increase in electron density with coordination number of neighboring Li ions (see an inset of Figure 14; four A-site cations are close to the oxide ion). In this figure, the radius of the sphere for the integration of differential electrons of 1.4 Å corresponds to the ionic radii of oxide ion.[35] As seen in the figure, the increase in electrons around oxide ion clearly showed liner relationships with the number of neighboring lithium ions. Thus, the electrons of inserted lithium transferred to neighboring oxide ion locally, and such a behavior would effectively neutralize strong electrostatic interaction arising from inserted lithium ion.

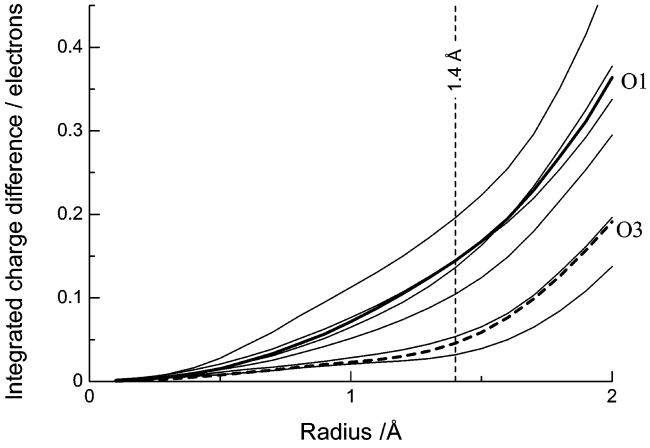

Figure 13. Variation of the differential electrons for each site as a function of integration radius. Differential electrons around (a) oxygen (thick-solid and thick-hatched line represents O1 and O3 site, respectively), (b) titanium, and (c) lanthanum.

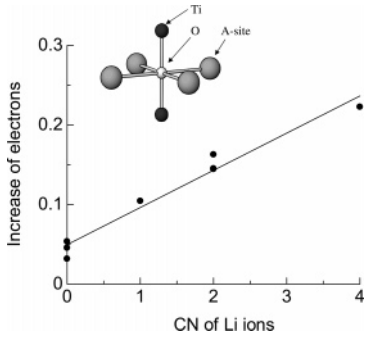

Figure 14. Variation of increase of electron around oxide ion with electrochemical lithium uptake as a function of coordination number (CN) of Li ions. The radii of spheres for differential electron integration are 1.4 Å. Inset picture shows the coordinated cations around oxide ion, two titanium ion as first neighbor and four coordinated A-site cations as second neighbor of oxide ion.

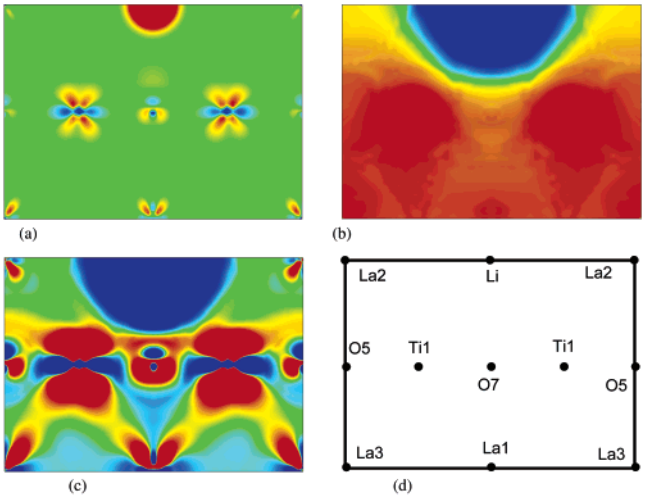

Figure 15. The differential map before and after lithium insertion: (a) electron density, red area indicates the increase of electron density and blue is vice versa; (b) the potential of electrons, blue area indicates the lower potential (or stable) for electron; (c) the correlation map, blue area indicates the increase of electron density where the potential of electron is stabilized, or vice verse; (d) the arrangement of ions for reference.

As indicated by both of experimental and computational results, the changes in electronic structure occurred not only at the titanium ion but also at the oxide ion. In particular, the electron structure around oxide ions seemed to be strongly

affected by the lithium ion itself. However, since the orbital level of Li 2s state is far from the Fermi level where the electron transfer mainly takes place. Hence, the contribution of lithium to the transfer at oxide ion is not via Li 2s−O 2p covalent orbital, but the other kind of interaction between Li and O, such as Coulombic potential. The potentials of the electron were calculated for VLTO and LLTO from the calculated electron distribution, and its difference were shown in Figure 12b. The blue part in the figure corresponds to the lowered potential area, or stabilized area for electrons after the lithiation. The figure shows that the area around lithium insertion site stabilized significantly, and the stabilization of the potential seemed to affect the neighboring oxide ion. The corresponding differential electron density map was also shown in Figure 12a and multiplied to the differential potential map. Figure 12c represents the results of multiplication. In this figure, blue area indicates the strong correlation between increase of the electron density and stabilization of the potential, and vice versa. The figure clearly implies that the increase of electron around oxide ion near insertion site (O7) ascribed to the stabilization of the potential. Therefore, the changes in electronic structure of oxide ions seem to be the variation of the potential introduced by Li ions with strong ionic character, since the changes in electronic structure at oxide ions through the insertion of Li is strongly dependent on the neighboring Li.

5. Conclusion

XAS measurement for electrochemical reaction in (Li,La)-TiO_3 system revealed that the oxidation states of La was unchanged through the electrochemical lithium insertion, while electronic structural change was observed around Ti and O ion. In particular, indication of changes in electronic structure around oxide ions is surprising despite of the fact that Ti ion belongs to the early TM system. Through the study on XAS for $Li_yLa_{(2-y)/3}TiO_3$ and ab initio calculation, it was revealed that the electronic structural change in Ti was ascribed to the electron content in the lattice, while that observed in oxygen seems to be strong interaction between oxygen and neighboring Li^+ ion indicated and the variation of the electronic structure could be understood not only by the framework of covalent or ionic bond type classification, but by the potential change in the lattice induced by the strong ionic character of lithium ion. Such a discussion would be widely applied to the other electrochemical systems, especially for lithium-ion-battery materials, because the concept of electrostatic interaction is known as the general subject in the solid-state materials.

Acknowledgment. M. Nakayama would like to thank to Japan Society for the Promotion of Science (JSPS) for financial support of this work. The La L_3-edge and Ti K-edge XAS experiments were performed at the Photon Factory with the approval of High Energy Accelerator Research Organization (Proposal No. 2002G254), and O K-edge XAS measurements were carried out at the UVSOR with the approval of Institute for Molecular Science (Proposal No.14-865). Figure 12 was drawn with VENUS developed by R. A. Dilanian and F. Izumi. Finally, the authors thank to the reviewer for helpful comments on a draft of this paper.

References and Notes

(1) Megahid, S.; Scrosati, B. *J. Power Sources* **1994**, *51*, 79. Scrosati, B. *Nature* **1995**, *573*, 557. Scrosati, B. *Electrochim. Acta* **2000**, *45*, 2461

(2) Wakihara, M.; Li, G.; Ikuta, H. *Lithium Ion Batteries*; Kodansha: Tokyo, 1998; Chapter 2.

(3) Ceder, G.; Aydinol, M. K.; Kohan, A. F. *Compt. Mater. Sci.* **1997**, *8*, 161. Aydinol, M. K.; Kohan, A. F.; Ceder, G.; Cho, K.; Joannopoulos, J. *Phys. Rev. B* **1997**, *56*, 1354. Aydinol, M. K.; Ceder, G. *J. Electrochem. Soc.*, **1997**, *144*, 3832. Ceder, G.; Chiang, Y.-M.; Sadoway, D. R.; Aydinol, M. K.; Jang, Y.-I.; Huang, B. *Nature* **1998**, *392*, 694. Mishra, S. K.; Ceder, G., *Phys. Rev. B.*, **1999**, *59*, 6120.

(4) Koyama, Y.; Kim, Y.-S.; Tanaka, I.; Adachi, H. *Jpn. J. Appl. Phys*. **1999**, *38*, 2024.

(5) Uchimoto, Y.; Sawada, H.; Yao, T. *J. Synchrotron Rad.* **2001**, *8*, 872. Uchimoto Y., Sawada, H.; Yao, T. *J. Power Sources* **2001**, *97*−*98*, 326.

(6) Kim, M.-G.; Lee, M.-K.; Shin, H.-J.; Lee, J.-M.; Lee, J.-S.; Yo, C.-H. *J. Phys. Chem. B* **2002**, *106*, 2526.

(7) Pauling, L. *The Nature of the Chemical Bond*, 3rd ed.; Cornell University Press: New York, 1960.

(8) Allred, A. L., *J. Inorg. Nucl. Chem.* **1961**, *17*, 215.

(9) Van der Ven, A.; Aydinol, M. K.; Ceder, G. *Phys. Rev. B* **1998**, *58*, 2975

(10) Nakayama, M.; Imaki, K.; Ra, W.; Ikuta, H.; Uchimoto, Y.; Wakihara, M. *Chem. Mater.* **2003**, *15*, 1728. Nakayama, M.; Ra, W.; Ikuta, H.; Uchimoto, Y.; Wakihara, M. *Electrochemistry* **2003**, *71*, 1025.

(11) Belous, A. G.; Novitskaya, G. N.; Polyanetskaya, S. V.; Gornikov, Yu. I. *Izvestiya Akademii Nauk SSSR, Neorg. Mater.* **1987**, *23*, 470.

(12) Inaguma, Y.; Chen, L.; Itoh, M.; Nakamura, T.; Uchida, T.; Ikuta, H.; Wakihara, M. *Solid State Commun.* **1993**, *86*, 689. Inaguma, Y.; Chen, L.; Itoh, M.; Nakamura, T. *Solid State Ionics* **1994**, *70/71*, 196. Itoh, M.; Inaguma, Y.; Jung, W. H.; Chen, L.; Nakamura, T. *Solid State Ionics* **1994**, *70/71*, 203.

(13) Fourquet, J. L.; Duroy, H.; Crosnier-Lopez, M. P. J. *Solid State Chem.* **1996**, *127*, 283.

(14) Harada, Y.; Ishigaki, T.; Kawai, M.; Kuwano, J.; *Solid State Ionics* **1998**, *108*, 407.

(15) Ibarra, J.; Varez, A.; Leon, C.; Santamaria, J. Torres-Martinez, L. M.; Sanz, J. *Solid State Ionics* **2000**, *134*, 219.

(16) Mazza, D.; Ronchetti, S.; Bohnké, O.; Duroy, H., Fourquet, J.-L. *Solid State Ionics* **2002**, *149*, 81. Bohnké, O.; Duroy, H.; Fourquet, J.-L.; Ronchetti, S.; Mazza, D. *Solid State Ionics* **2002**, *149*, 217.

(17) Shan, Y.-J.; Chen, L.; Inaguma, Y.; Itoh, M.; Nakamura, T. *J. Power Sources* **1995**, *54*, 397.

(18) Bohnké, O.; Bohanke, C.; Fourquet, J.-L. *Solid State Ionics* **1996**, *91*, 21.

(19) Chen, C.-H.; Amine, K. *Solid State Ionics* **2001**, *144*, 51.

(20) Bohnké, O.; Emery, J.; Fourquet, J.-L.; Badot, J.-C. *Recent Res. Dev. Solid State Ionics* **2003**, *1*, 47.

(21) Inaguma, Y.; Katsumata, T.; Itoh, M.; Morii, Y. *J. Solid State Chem.* **2002**, *166*, 67.

(22) Yoshioka, H. *J. Am. Ceram. Soc.* **2002**, *85*, 1339.

(23) Emery, J.; Bohnké, O.; Fourquet, J.-L.; Buzaré, J.-Y.; Florian, P.; Massiot, D. *J. Phys.: Condens. Matter* **1999**, *11*, 10401.

(24) Kohn, W.; Sham, L. J. *Phys Rev.* **1965**, *140*, 1133.

(25) For example, Sjöstedt, E.; Nordström, L.; Singh, D. J. *Solid State Commun.* **2000**, *114*, 15. Cottenier, S. *Density Functional Theory and the family of (L)APW-Methods: A Step-by-Step Introduction*; Instituut voor Kern- en Stralingsfysica, K. U. Leuven: Belgium, 2002 (to be found at http:// www.wien2k.at/reg_user/textbooks).

(26) Pewdew, J. P.; Burke, K.; Ernzerhof, M. *Phys. Rev. Lett.* **1996**, *77*, 3865.

(27) Blaha, P.; Schwarz, K.; Sorantin, P.; Trickey, S. B. *Comput. Phys. Commun.* **1990**, *59*, 399. Blaha, P.; Schwarz, K.; Madsen, G. K. H.; Kvasnicka, D.; Luitz, J. *WIEN2k, Vienna University of Technology, An Augmented Plane Wave + Local Orbitals Program for Calculating Crystal Properties*, revised edition; 2001 (for further details see, for example, the documentation at the URL: http://www.wien2k.at)

(28) Ceder G. *Science* **1998**, *280*, 15.

(29) Zaanen, J.; Sawatzky, G. A.; Allen, J. W. *Phys. Rev. Lett.* **1985**, *55*, 418.

(30) Arima, T.; Tokura, Y.; Torrance, J. B. *Phys. Rev. B* **1993**, *48*, 17006.

(31) Okimoto, Y.; Katsufuji, T.; Okada, Y.; Arima, T.; Tokura, Y. *Phys. Rev. B* **1995**, *51*, 9581.

(32) Meijer, G. I.; Henggeler, W.; Brown, J.; Becker, O.-S.; Bednorz, J. G.; Rossel, C.; Wachter, P. *Phys. Rev. B* **1999**, *59*, 11832

(33) Hamada, N.; Sawada, H.; Solovyev, I.; Terakura, K. *Physica B* **1997**, *11*−*13*, 237.

(34) Katsumata, T.; Inaguma, Y.; Itoh, M.; Kawamura, K. *Chem. Mater.* **2002**, *14*, 3930.

(35) Shannon, R. D. *Acta Crystallogr*. **1976**, *A32*, 751.